JACS
JOURNAL OF THE AMERICAN CHEMICAL SOCIETY
pubs.acs.org/JACS
Article

Anchoring Side Chains to Carbonate Groups for Reviving Stable Polycarbonate-Based Solid-State Lithium Metal Batteries

Hantao Xu,[▽] Wei Deng,[▽] Jingyuan Yu,[▽] Lei Shi, Wenwei Zhang, Juncai Long, Chaobin He,* and Lin Xu*

Cite This: J. Am. Chem. Soc. 2025, 147, 16154−16163
Read Online
ACCESS | Metrics & More | Article Recommendations | Supporting Information

ABSTRACT: Polycarbonate-based electrolytes are ideal electrolytes for solid-state lithium metal batteries (LMBs) due to their wider electrochemical windows and considerable ionic conductivities compared with conventional solid polymer electrolytes. However, polycarbonates encounter severe interfacial side reactions with lithium metal, leading to the interfacial degradation of polymers. Herein, a spontaneously formed restricted conformation is designed via the in situ anchoring of side chains to suppress the interfacial degradation of polycarbonate-based electrolytes. The restricted conformation enables the side chains to shield and protect the degradable ester bonds of cyclic carbonates, suppressing contact and interfacial degradation between polycarbonates and lithium metal anodes. As a proof of concept, the protected polycarbonate-based electrolyte demonstrates a stable cycling capability of the Li/Li cell beyond 1000 h at a current density of 0.5 mA cm^{-2}, and the assembled $LiNi_{0.8}Co_{0.1}Mn_{0.1}O_2$/Li pouch cell also achieves similar improvement in cycling performance. This work indicates that the strategy of constructing restricted conformations via anchoring side chains is a feasible avenue for fabricating highly stable polycarbonate-based solid-state LMBs.

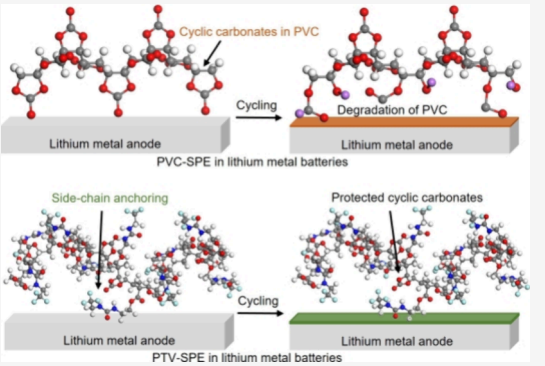

1. INTRODUCTION

Lithium metal batteries (LMBs) are attracting extensive interest due to their low reduction potential and high theoretical specific capacity.[1,2] However, the applications of LMBs are still limited by short lifespans[3] and safety hazards,[4] mainly due to the use of active lithium metal and large amounts of highly flammable liquid electrolytes.[5] To overcome this challenge, solid polymer electrolytes (SPEs) are considered as the viable candidate for LMBs due to their higher safety, nonvolatility, good processability and flexibility.[6] However, the widely reported poly(ethylene oxide) (PEO)-based solid polymer electrolyte encounters the limitation of a narrow electrochemical window,[7,8] while other solid polymer electrolytes such as polyvinylidene difluoride (PVDF),[9] poly(methyl methacrylate),[10] and polyacrylonitrile[11] exhibit poor Li^+ transport capability.[12] These challenges hinder further development and application of solid polymer electrolytes.

To overcome these issues, polycarbonate-based solid polymer materials such as polyethylene carbonate (PEC),[13] polypropylene carbonate (PPC),[14] and polyvinylene carbonate (PVC)[15] have been reported as solid-state electrolytes for LMBs due to their considerable ionic conductivities and wide electrochemical windows.[16] However, challenges still remain in the practical application of polycarbonate-based solid polymer electrolytes in LMBs.[17] The first challenge is the poor interfacial contact between rigid polycarbonate-based solid polymer electrolytes and the electrodes, which increases the interfacial impedance during cycling.[18] The main reason behind this is the nonuniform interfacial contact due to the high glass transition temperature (Tg) of the polycarbonate-based electrolytes. To address this issue, several works have been reported such as the use of in situ polymerization,[19] introducing hyperbranched polycarbonates with low Tg, and the addition of plasticizers[20] to effectively reduce the interfacial impedance of polycarbonate-based LMBs and improve the cycling stability. Another more serious challenge is the severe interfacial reaction of polycarbonate-based solid polymer electrolytes in contact with lithium metal anodes (LMAs) during cycling, leading to the degradation of ester bonds in the polycarbonate-based polymer matrix (Figure 1a).[21] For example, it was reported that the interfacial degradation of PVC-based polymer electrolytes first receives an electron from the LMA and breaks the C−O bond of ester bonds in the cyclic carbonate structure.[22] Subsequently, the polymer receives another electron, resulting in the breaking of the

Received: January 14, 2025
Revised: March 9, 2025
Accepted: April 22, 2025
Published: May 1, 2025

https://doi.org/10.1021/jacs.5c00760
J. Am. Chem. Soc. 2025, 147, 16154−16163

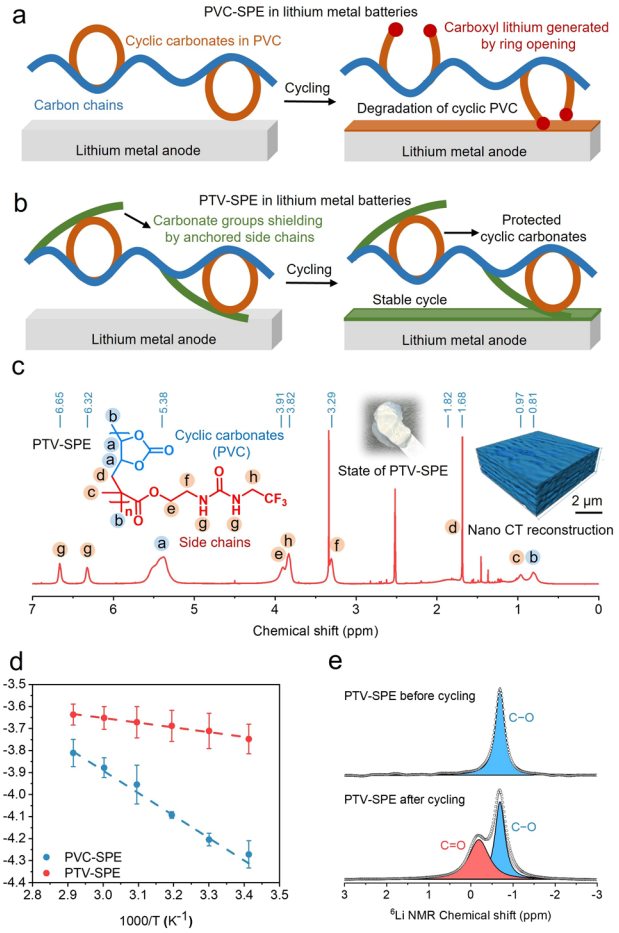

Figure 1. Design and characterization of the solid-state electrolyte. (a) Ring-opening degradation of PVC-SPE on the surface of lithium metal. (b) Suppression of interfacial degradation by the restricted conformation via anchoring side chains. (c) ^{1}H NMR spectrum of the synthesized PTV-SPE (insets are an optical photograph and the 3D nano CT reconstruction of the PTV-SPE). (d) Temperature-dependent curve of the ionic conductivities of PTV-SPE. (e) ^{6}Li NMR spectra of PTV-SPE before and after cycling.

C−O bond on the other side of the carbonyl carbon.[22] This degradation of ester bonds cuts off the transport paths of Li^+, causing increases in internal impedances within the cells. Finally, it degrades into small-molecule byproducts that limit the cycling performance of polycarbonate-based LMBs and pose safety hazards.[21] So far, the degradation of PVC has not been effectively addressed, hindering the applications of polycarbonate-based solid polymer electrolytes.[23]

Here, we report a side-chain anchoring design to enhance the chemical stability of PVC-based solid polymer electrolytes toward LMAs, where trifluoromethyl methacrylate-based side chains are in situ anchored to the PVC backbone. This design allows the side chains to spontaneously form a stable restricted conformation through hydrogen-bonding anchoring between the rigid main chains and flexible side chains. Furthermore, the restricted conformation shields and protects the ester bonds of cyclic carbonate structures, thus suppressing the direct contact of the PVC ester bond with LMAs and improving the anodic chemical stability of cyclic carbonate structures. Our strategy effectively limits the interfacial side reactions of polycarbonate-based solid polymer electrolytes and reduces the interfacial degradation of the polymer electrolytes (Figure 1b). As a result, the prepared solid polymer electrolyte with restricted conformation demonstrates stable cycling performance of a symmetrical Li/Li cell beyond 1000 h, and the corresponding $LiFePO_4$/Li cell exhibits stable cycling capability for over 1000 cycles. Similar enhanced performance of the full cell is also realized in the 0.8 Ah $LiNi_{0.8}Co_{0.1}Mn_{0.1}O_2$/Li pouch cell, which demonstrates that our design strategy of restricted conformation via anchoring side chains provides a feasible approach to constructing stable polycarbonate-based LMBs.

2. RESULTS AND DISCUSSION

2.1. Design and Preparation of the Side-Chain-Anchored Polymer Electrolyte. A ureido-based monomer named 2-(3-(2,2,2-trifluoroethyl)ureido)ethyl methacrylate (TUEM) was synthesized through nucleophilic addition of 2-isocyanatoethyl methacrylate (Figure S1). The corresponding side-chain-anchored polymer electrolyte denoted poly(TUEM-VC)-SPE (PTV-SPE) was prepared in situ by copolymerization of vinylene carbonate (VC) and TUEM (Figure S2). The results of the nuclear magnetic resonance (NMR) spectra indicate that the side chains (TUEM segments) are successfully attached to the PVC main chains (Figures 1c and S3a). The ^{1}H−^{1}H correlation spectroscopy (^{1}H−^{1}H COSY) experiment reveals coupling signals between the polycarbonate main chain and the side chain structures of PTV-SPE (Figure S3b), indicating the existence of the copolymer structure shown in Figure 1c. In addition, the disappearance of the stretching vibration absorption peak of the C═C bonds located at 1618 cm^{-1} of TUEM and 1565 cm^{-1} of VC in the Fourier transform infrared spectrometer (FTIR) spectra (Figure S4) suggests that the prepared semitransparent solid-state electrolyte (Figure 1c, inset) is PTV-SPE.[20,24] The result of gel permeation chromatography indicates that the molecular weight (M_w) of PTV-SPE is 1.42 × 10^5 g mol^{-1} (Figure S5). The thermogravimetric experiment indicates that the prepared PTV-SPE has a high polymerization conversion rate and very little residual liquid monomer (Figure S6). Nano CT reconstruction and the scanning electron microscope (SEM) image show that the in situ prepared PTV-SPE membrane exhibits a flat and uniform morphology (Figure 1c inset, Figure S7), indicating good uniformity of in situ preparation of PTV-SPE. The XRD pattern shows a broad peak around 20°, indicating the almost amorphous nature of PTV-SPE (Figure S8). To investigate the optimal copolymerization ratio of this solid-state electrolyte, PTV-SPE electrolytes with different ratios were prepared to observe their states and test their ionic conductivities. The result shows that PTV-SPE with a copolymerized TUEM mass fraction of 15.5 wt % exhibits good solid-state properties and superior ionic conductivity, making it the optimal ratio for the following experiments (Figures S9 and S10). The in situ prepared PTV-SPE with this mass ratio exhibits an enhanced ionic conductivity (σ) of 2.22 × 10^{-4} S cm^{-1} at 25 °C and a low activation energy (E_a) of 0.04 eV, compared to that of homopolymer PVC-SPE with the σ of 6.55 × 10^{-5} S cm^{-1} and E_a of 0.20 eV (Figure 1d). ^{6}Li NMR results of PTV-SPE before and after 50 cycles using ^{6}Li metal as electrodes reveal that the enhancement in ionic conductivity of PTV-SPE is mainly due to the contribution of the C═O structures (−0.18 ppm) of the cyclic carbonate structures and side chains to Li^+ transport (Figure 1e).[25] In addition, PTV-SPE shows a higher onset potential of oxidative decomposition (4.5 V) than that of (4.1 V) PVC-SPE (Figure S11) and exhibits a stress modulus

https://doi.org/10.1021/jacs.5c00760
J. Am. Chem. Soc. 2025, 147, 16154−16163

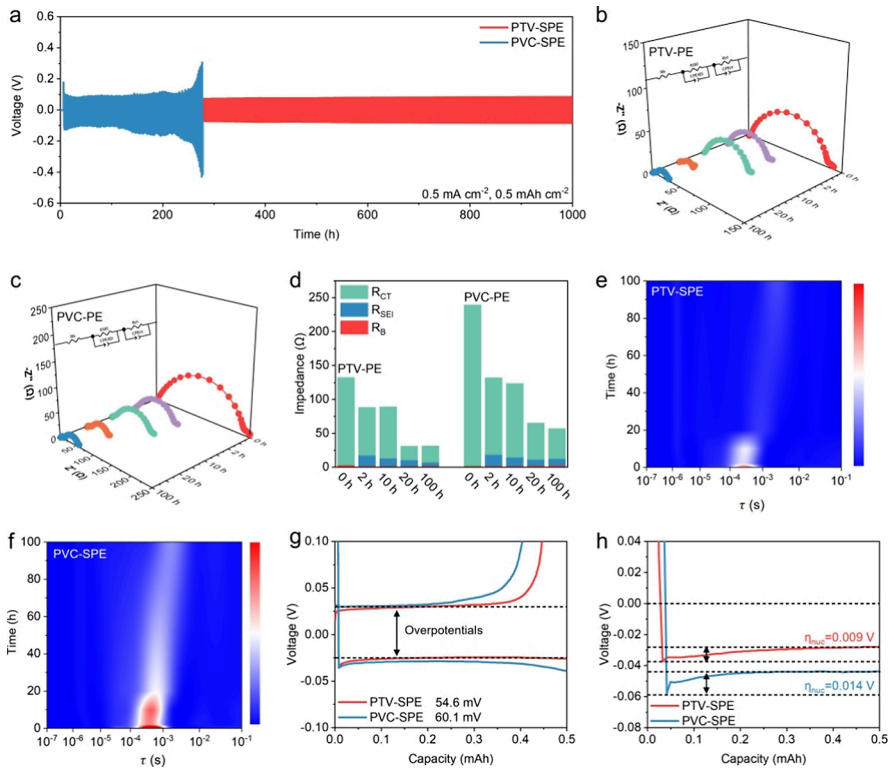

Figure 2. Test of interfacial stability. (a) Voltage profiles of the Li/Li symmetric cells with PTV-SPE and PVC-SPE. (b) Nyquist plots of the impedance of Li/PTV-SPE/Li at different cycles. (c) Nyquist plots of the impedance of Li/PVC-SPE/Li at different cycles. (d) Fitting results of interfacial impedances of Li/Li cells assembled with PTV-SPE and PVC-SPE at different cycles. (e) Corresponding DRT transformation of the Li/PTV-SPE/Li cell. (f) Corresponding DRT transformation of the Li/PVC-SPE/Li cell. (g) Galvanostatic discharge/charge profiles of Cu/Li cells with PTV-SPE and PVC-SPE. (h) Corresponding nucleation and plateau overpotentials of the first Li deposition in Cu/Li cells based on PTV-SPE and PVC-SPE.

exceeding 94.5 N mm^{-2} (Figure S12). Furthermore, PTV-SPE also shows a high lithium ion transference number (t_{Li}^+) of 0.73 (Figure S13a), which is higher than that of homopolymer PVC-SPE (t_{Li}^+ = 0.47), indicating the potential existence of hydrogen-bonded interactions between the PTV polymer and $TFSI^-$ anions (Figure S13b). The above evidence suggests that PTV-SPE exhibits high mechanical-chemical stability, large t_{Li}^+, and superior ionic conductivity, which illustrates the potential for application in LMBs.

2.2. Evaluation of Side Reactions and Interfacial Degradation of PVC-Based Solid Polymer Electrolytes. To investigate the performance of PTV-SPE, symmetrical Li/Li cells and Cu/Li cells were assembled and evaluated. The Li/PTV-SPE/Li cell demonstrates an overpotential of 85 mV at a current density of 0.5 mA cm^{-2} for more than 1000 h, exhibiting stable voltage profiles (Figure 2a). In comparison, the Li/PVC-SPE/Li cell delivers unstable fluctuant voltage profiles with large overpotentials of up to 256 mV at 270 h, indicating that the electrolyte or interface is unstable without side chain protection. To clarify the source, in situ electrochemical impedance spectroscopy was used to evaluate the impedance evolutions at different cycles (Figure 2b,c). The R_b and R_{ct} (2.3 and 23.9 Ω at 100 h) of the Li/PTV-SPE/Li cell remain stable and low level of interfacial impedances before 100 h, while the Li/PVC-SPE/Li cell shows a slightly high R_b (2.9 Ω) and a large R_{ct} (44.3 Ω) before 100 h (Figure 2d). This suggests that the Li/PVC-SPE/Li cell experiences more severe interfacial side reactions than PTV-SPE, which results in varying increases in both R_b and R_{ct}. The analysis of EIS data using the relaxation time semiquantitative distribution (DRT) method shows similar results. In the region of electrolyte/Li interface ($10^{-4} < \tau < 10^{-2}$ s),[26] the peak in PTV-SPE rapidly decreases and reaches stability, while the peak in PVC-SPE still maintains high strength, indicating that the Li/PVC-SPE/Li cell has a large interfacial impedance that may be caused by interfacial side reactions (Figure 2e,f). Furthermore, the PTV-based cell delivers a high critical current density of >2 mA cm^{-2} (Figure S14) and a high exchange current density (i_0) of 1.21 mA cm^{-2} (Figure S15), in contrast to multiple unstable fluctuations at low currents and low i_0 of PVC-SPE. In addition, the Cu/PTV-SPE/Li cell exhibits higher Coulombic efficiency than PVC-SPE (Figure S16), and the overpotential at 50 cycles is 54.6 mV, lower than 60.1 mV of the PVC-SPE counterpart (Figure 2g). In addition, Cu/PTV-SPE/Li demonstrates better lithiophilicity with a low η_{nuc} of 0.009 V at the first cycle, compared to the high η_{nuc} (0.014 V) of the PVC-SPE-based cell, suggesting favorable conditions for uniform Li deposition and suppression of side reactions in PTV-SPE (Figure 2h).[27] All the above results indicate that PTV-SPE demonstrates superior interfacial stability toward lithium metal, but the reasons for the improved stability still need to be investigated.

It is reported that the main reason for the poor interfacial stability of polycarbonate-based solid polymer electrolytes is the degradation of the polymers on the surface of the lithium metal. The interfacial degradation of PVC-SPE at the surface of lithium metal may be similar to that of cyclic carbonate molecules, which is decomposed by accepting an electron from

https://doi.org/10.1021/jacs.5c00760
J. Am. Chem. Soc. 2025, 147, 16154−16163

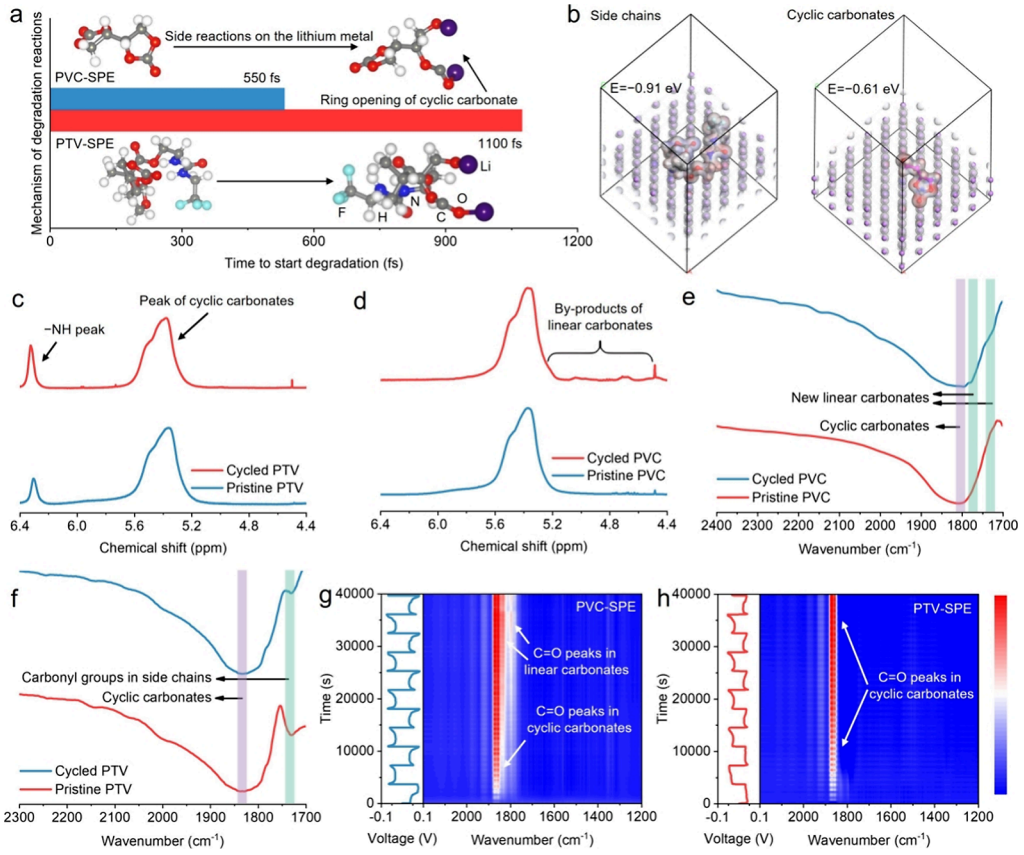

Figure 3. Degradation mechanism of polycarbonate-based electrolytes. (a) Degradation reaction mechanism based on AIMD simulations of PTV-SPE and PVC-SPE on the surface of LMAs. (b) The adsorption energies of side chain and cyclic carbonate structure of PTV-SPE absorbed on LMAs. (c) ^{1}H NMR spectra of the precipitation products of PTV-SPE before and after cycling. (d) ^{1}H NMR spectra of the precipitation products of PVC-SPE before and after cycling. (e) FTIR spectra of the precipitation products of PVC-SPE before and after cycling. (f) FTIR spectra of the precipitation products of PTV-SPE before and after cycling. (g) In situ ATR-FTIR of the degradation of polymers between PVC-SPE and LMA. (h) In situ ATR-FTIR of degradation of polymers between PTV-SPE and LMA.

the surface of LMA and breaking the C−O bond between the carbonyl C atom and the O atom on a cyclic carbonate structure.[22] The ab initio molecular dynamics (AIMD) method was used to demonstrate this degradation process.[28] The results of AIMD simulations show that PVC-SPE undergoes an initial ring-opening reaction of the cyclic carbonate structure after 550 fs of contact with lithium metal, generating a degradation product of organic lithium compounds. In contrast, PTV-SPE degrades only after 1100 fs of contact with lithium metal, which is attributed to the protection of the cyclic carbonate structures by the effect of restricted conformation (Figure 3a). Moreover, the adsorption energy of side chains with LMA (−0.91 eV) is lower than that of cyclic carbonate structures (main chains) with LMA (−0.61 eV) in PTV-SPE (Figure 3b). This indicates that the side chains are more inclined to adsorb on the surface of LMA, inhibiting the degradable cyclic carbonate structures and improving the chemical stability of the cyclic carbonate structures. To further confirm the side reactions of PVC-SPE at the interface, the precipitation products of the polymer electrolytes before and after 50 cycles of Li/Li cells were characterized by FTIR and NMR. Compared to the ^{1}H NMR spectrum of PVC-SPE before cycling, there are additional broad peaks at 4.5−5.1 ppm after cycling, while there are no new peaks in the ^{1}H NMR spectrum of PTV-SPE after cycling (Figure 3c,d).[29] These new peaks at the high field are the hydrogen atoms on the linear carbonate structures after interfacial ring-opening reactions.[29] In addition, FTIR results also showed that new C═O shoulder peaks at 1779.6 and 1735.2 cm^{-1} are observed in the cycled PVC-SPE (Figure 3e), which can be attributed to the stretching vibration of C═O in linear carbonate structures after ring-opening side reactions.[29] While there is no change in the FTIR spectra of PTV-SPE before and after cycling (Figure 3f), there is only pristine stretching vibration of C═O in cyclic carbonates (1841.1 cm^{-1}) and vibration of linear C═O in side chains (1729.3 cm^{-1}).[30] The above results suggest that the interfacial side reactions in PTV-SPE are much less than those in PVC-SPE, resulting in a more stable chemical structure of cyclic carbonates in PTV-SPE during cycling. Furthermore, in situ FTIR spectra were used to characterize the degradation of cyclic carbonate structures in polymer electrolytes in real-time. It can be seen that the linear C═O stretching vibration peak belonging to the byproduct of interfacial reactions at 1786.5 cm^{-1} gradually appears during cycling in PVC-SPE, in addition to the pristine C═O stretching vibration peak of cyclic carbonates at 1849.1 cm^{-1} (Figure 3g).[30] In contrast, there is no significant change in the in situ FTIR spectra of the PTV-based cell during cycling (Figure 3h), indicating the enhanced chemical stability of cyclic carbonate structures in PTV-SPE.

SEM, X-ray photoelectron spectroscopy (XPS) sputtering, and 3D time-of-flight secondary-ion mass spectrometry (TOF-SIMS) analyses on the surface of lithium metal disassembled from 50-cycle Li/Li cells were also characterized. The top-view

https://doi.org/10.1021/jacs.5c00760
J. Am. Chem. Soc. 2025, 147, 16154−16163

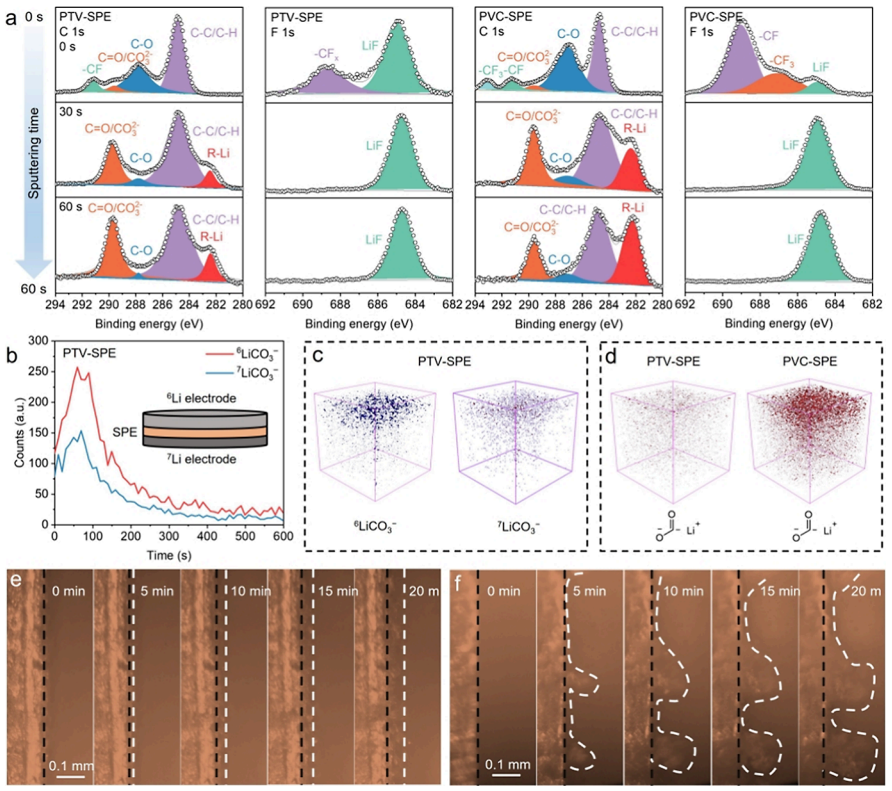

Figure 4. Evolution of interfacial compositions and morphologies. (a) XPS spectra of cycled PTV-based SEI and PVC-based SEI at different sputtering depths. (b) TOF-SIMS depth profiles of $^{6}LiCO_3^-$ in PTV-based and PVC-based SEIs after cycling (inset is the asymmetric $^{6}Li/^{7}Li$ cell assembled for cycling). (c) 3D TOF-SIMS mappings of $^{6}LiCO_3^-$ for the cycled LMA toward PTV-SPE. (d) 3D TOF-SIMS mappings of organic carbonyl lithium fragments for the cycled LMA toward PTV-SPE and PVC-SPE. (e) Lithium deposition morphologies of the Li/PTV-SPE/Li cell after different times. (f) Lithium deposition morphologies of the Li/PVC-SPE/Li cell after different times.

SEM image shows that a flat and homogeneous surface is observed on the LMA of the PTV-based cell, while the LMA surface of the PVC-based cell shows an inhomogeneous deposition morphology with pore-like features (Figure S17). In the XPS C 1s spectra (0 s sputtering), the SEI surface toward PTV-SPE exhibits reduced C−O (287.8 eV) and $-CF_3$ (293.1 eV) than that of PVC-SPE (Figure 4a), indicating that PTV-SPE can suppress the degradation of polycarbonate structures and promote the reduction of trifluoromethyl structures.[20] In the C 1s spectra of the PVC-based cell, a new peak (282.4 eV) of organo-lithium compounds appears after 30 s sputtering, mainly from the byproducts of lithium alcoholate and lithium carboxylate generated after the interfacial reaction of cyclic carbonates with lithium metal.[31] While in the PTV-based cell, the amount of R−Li byproduct is less than that of PVC-SPE at 30 and 60 s sputtering, demonstrating the enhanced interfacial stability of PTV-SPE. In addition, PTV-based SEI has more decomposed LiF (685.0 eV) in the different depths of XPS F 1s spectra (Figure 4a), which is consistent with the results of the C 1s spectra.[32] Additionally, the corresponding XPS elemental composition results reveal that at 0 s sputtering time, the LMA with PTV-SPE exhibits a lower C content (39.3%) and a higher F content (19.3%). In contrast, the PVC-SPE sample shows a higher C content (52.3%) and a lower F content (6.0%), with a similar trend observed across different sputtering depths (Table S1). This finding suggests that anchoring the side chains of PTV-SPE reduces the degradation of polycarbonate in the LMA and promotes the formation of an F-rich interphase through the reduction of fluorinated side chains. Furthermore, the ^{6}Li and ^{7}Li electrodes were used to assemble an asymmetric $^{6}Li/^{7}Li$ cell for clarification of interfacial side reactions (Figure 4b, inset). The TOF-SIMS analyses show that the product of interfacial side reactions ($LiCO_3^-$) on the ^{6}Li electrode is mainly dominated by $^{6}LiCO_3^-$ after 50 cycles (Figure 4b,c). It indicates that the electrolyte is degraded mainly by a ring-opening reaction of the ^{6}Li metal on the LMA, rather than by $^{7}Li^+$ in the lithium salt. In addition, the 3D mappings and corresponding depth profiles of TOF-SIMS analyses show that the distribution of interfacial degradation products (organic carbonyl lithium fragments and $LiCO_3^-$) in PTV-based SEI is significantly lower than those in PVC-SPE (Figures 4d and S18), which suggests that PTV-SPE effectively suppresses the interfacial side reaction. In addition, the formation of interfacial dendrites on the surface of LMAs can be confirmed by observing the Li^+ deposition of the symmetric Li/Li cells through an in situ optical microscope. Under the current density of 2 mA cm^{-2}, the cross-sectional images of PTV-based LMA show homogeneous and dense lithium deposition after 20 min of lithium deposition (Figure 4e). In contrast, PVC-based LMA presents much more uneven lithium deposition and serious formation of lithium dendrites just after 5 min and even worsens at 20 min (Figure 4f). These findings illustrate that PTV-SPE can achieve homogeneous Li deposition and construct stable and dense SEI, which can be ascribed to the reduced interfacial side reactions between the polymer electrolyte and LMA.

2.3. Formation of Restricted Conformation via Anchoring Side Chains. To elucidate the mechanism behind the highly interfacial stability of PTV-SPE, density functional theory (DFT) calculations were used to optimize the

https://doi.org/10.1021/jacs.5c00760
J. Am. Chem. Soc. 2025, 147, 16154−16163

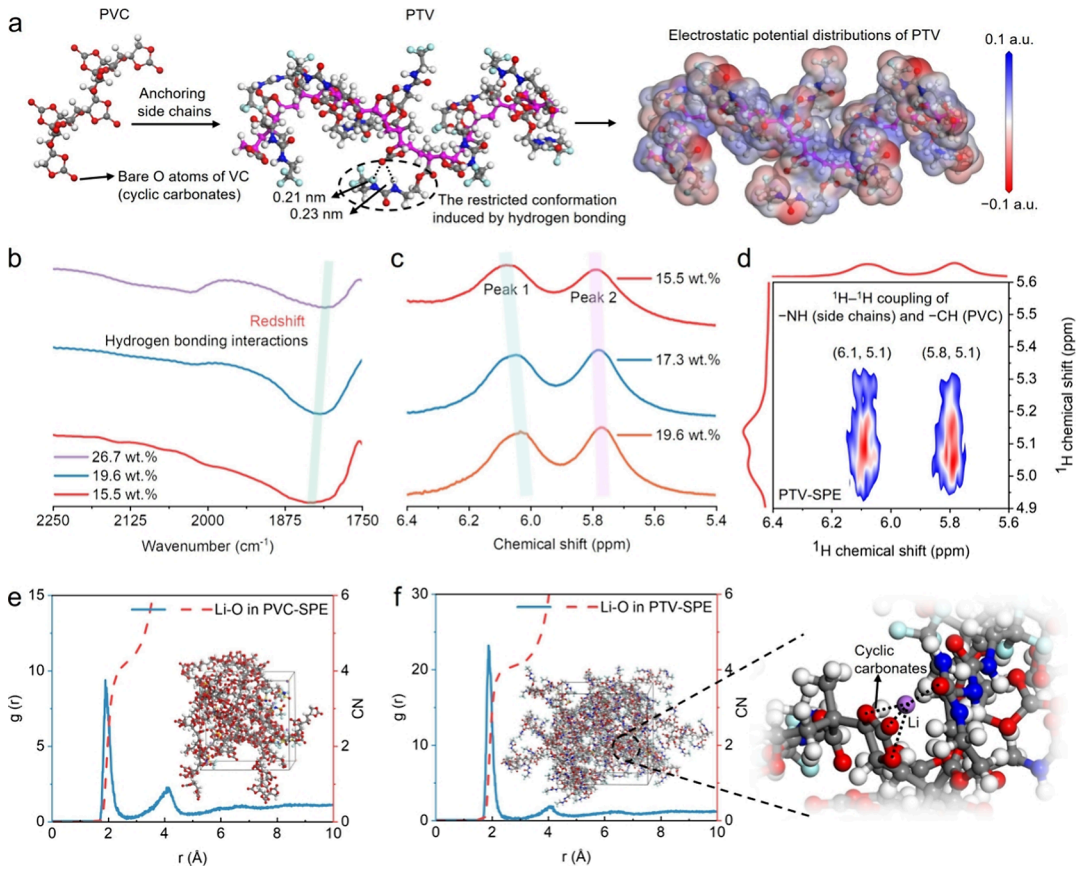

Figure 5. Characterization of the restricted conformation. (a) DFT model after optimization from the calculations and the electrostatic potential map of the PTV polymer. (b) FTIR spectra of PTV-SPE at different percentages of side chains. (c) ^{1}H NMR spectra of PTV-SPE at different percentages of side chains. (d) 2D ^{1}H−^{1}H NOESY spectrum of PTV-SPE. (e) Calculated RDF curves and coordination numbers in PVC-SPE (inset is the typical snapshot of PVC-SPE). (f) Calculated RDF curves and coordination numbers in PTV-SPE (insets are the typical snapshot of PTV-SPE and the partially enlarged view of the solvation structure of PTV-SPE).

molecular structure of the PTV polymer (Figure 5a). It is observed that the side-chain engineering changes the original straight chain morphology of the rigid cyclic carbonate-based main chain, as the flexible side chains form entanglement with the rigid main chain. More precisely, the PTV polymer spontaneously builds a helical polymer conformation and a special restricted conformation due to hydrogen-bonding interactions between the flexible side chains and rigid main chains. The measured lengths of hydrogen bonds are 0.21 and 0.23 nm. This special restricted conformation shields and protects the vulnerable cyclic carbonate structure that is prone to ring-opening degradation on the surface of LMA. To corroborate the DFT results, FTIR and NMR spectra were used to clarify the structure of the restricted conformation. As the percentage of side chains increases from 15.5 to 26.7 wt % in the single chain of PTV-SPE, the stretching band of C═O in FTIR spectra shifts from 1832.5 cm^{-1} toward a lower wavenumber of 1806.1 cm^{-1}, suggesting potential hydrogen-bonding interactions (Figure 5b).[33] In addition, the results of ^{1}H NMR spectra indicate that the double peak of −NH in side chain structures moves from 5.76 and 6.03 ppm to 5.80 and 6.07 ppm toward the downfield as the percentage of side chains decreases from 19.6 to 15.5 wt % (Figure 5c).[20] This suggests that −NH is influenced by hydrogen-bonding interactions, which leads to the deshielding effect of hydrogen atoms. In our previous work, it was determined that −NH in the trifluoroethyl ureido methacrylate structures only exhibits a single peak at 5.7 ppm in ^{1}H NMR.[20] The reason for the double peaks of −NH in PTV-SPE is due to the formation of a stable restricted conformation through hydrogen-bonding anchoring, leading to different chemical environments for the two−NH on the same ureido structures. Furthermore, the spatial correlations induced by the hydrogen-bonding interaction were further characterized by ^{1}H−^{1}H nuclear Overhauser effect spectroscopy (^{1}H−^{1}H NOESY) experiments. The ^{1}H−^{1}H NOESY experiment shows clear signals of coupling interaction in (6.1, 5.1 ppm) and (5.8, 5.1 ppm), in which the coupling between −CH of cyclic carbonate structures and −NH of side chains can be observed, indicating the closer spatial distance of cyclic carbonate structures and side chains caused by the formation of restricted conformation (Figure 5d). Moreover, low-molecular-weight PTV-SPE (7000 g mol^{-1}, at a higher concentration) was prepared for FTIR spectroscopy to distinguish between intramolecular and intermolecular hydrogen bonding (Figure S19a). The position of the C═O peak at 1832.5 cm^{-1} of the high-concentration PTV-SPE is almost unchanged compared to the low-concentration and also high-molecular-weight PTV-SPE (Figure S19b), indicating that the hydrogen-bonding interaction is almost concentration-independent. This suggests that intramolecular hydrogen bonding is dominant, while the limited intermolecular hydrogen bonding also contributes to side-chain anchoring.[34]

https://doi.org/10.1021/jacs.5c00760
J. Am. Chem. Soc. 2025, 147, 16154−16163

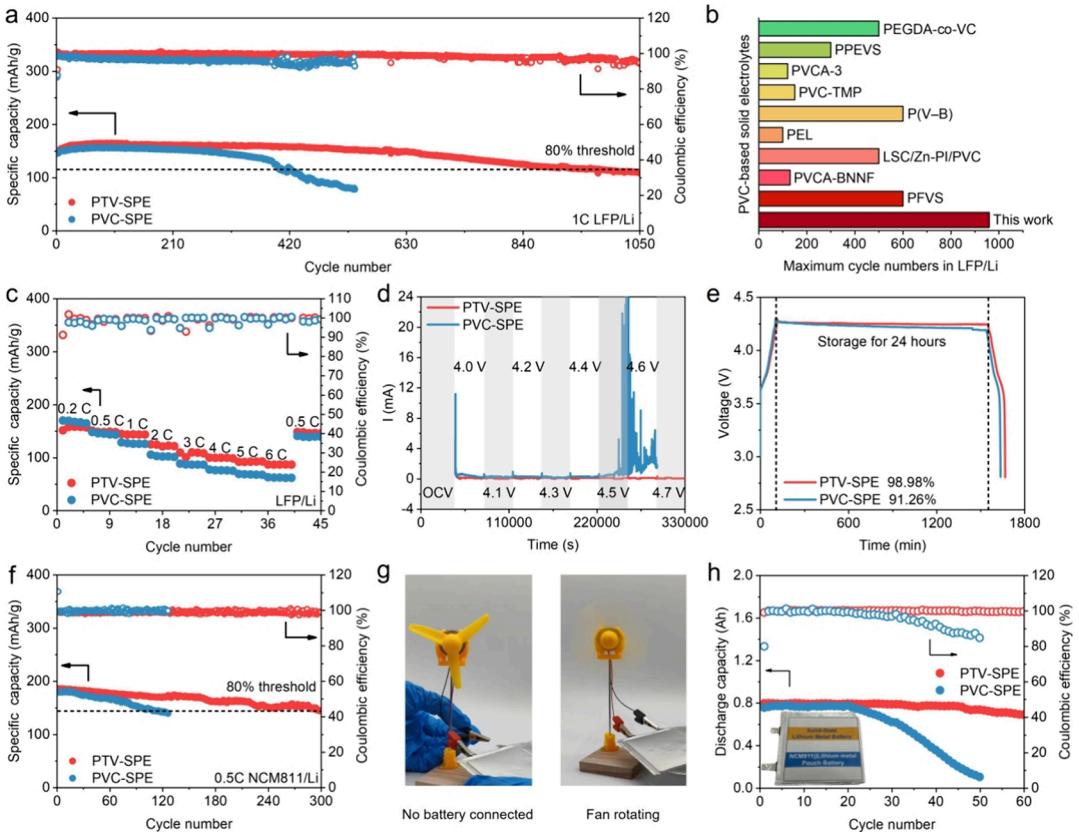

Figure 6. Construction of solid-state cells. (a) Cycling performance of $LiFePO_4$/Li cells with PTV-SPE and PVC-SPE at 0.5 C. (b) Comparison between $LiFePO_4$/PTV-SPE/Li and previously reported excellent $LiFePO_4$/PVC-based SPE/Li cells with a mass loading of more than 2 mg cm^{-2}, operating at room temperature, and a cutoff capacity retention rate of over 80% (PEGDA-*co*-VC;[35] PPEVS;[36] PVCA-3;[37] PVC-TMP;[38] P(V−B);[39] PEL;[40] LSC/Zn−PI/PVC;[41] PVCA-BNNF;[42] PFVS[43]). (c) Rate performance of $LiFePO_4$/Li cells using PTV-SPE and PVC-SPE at different rates. (d) Electrochemical floating curves of NMC811/PTV-SPE/Li and NMC811/PVC-SPE/Li cells at different voltages. (e) Self-discharge curves of NMC811/PTV-SPE/Li and NMC811/PVC-SPE/Li cells for 24 h. (f) Cycling performance of NCM811/Li cells using PTV-SPE and PVC-SPE at 0.5 C. (g) Demonstration of the NMC811/PTV-SPE/Li pouch battery operated fan. (h) Cycling performance of the 0.8 Ah NCM811/Li metal pouch cell of PTV-SPE and PVC-SPE at 0.5 C (inset is the optical photograph of the NCM811/PTV-SPE/Li metal pouch cell).

In addition, molecular dynamics (MD) was conducted to acquire deeper insights into the solvation structure of solid polymer electrolytes. The solvation structures, radial distribution functions (RDFs, $g(r)$), and coordination numbers (CNs) of PVC-SPE and PTV-SPE were calculated. In PVC-SPE, the dominant peak of the first Li^+ solvation shell of Li−O appears at 0.2 nm (Figure 5e), which is closer to that of PTV-SPE (Figure 5f). In addition, the CN of O in the first Li^+ solvation shell decreased from 4.2 to 4.0 after side-chain engineering, suggesting that the formation of a restricted conformation reduces coordination and promotes the transport of Li^+ (Figure 5e,f). Furthermore, the localized enlarged view of the solvation structure shows that Li^+ is mainly coordinated to the O atoms of the cyclic carbonate structures, indicating that Li^+ transport is mainly contributed to by the cyclic carbonate structures (Figure 5f). Interfacial degradation of the cyclic carbonate structure reduces the lithium transport sites of the polycarbonate polymers. These experiments and simulation results indicate that the formed restricted conformation can shield the vulnerable cyclic carbonate structures to prevent them from direct contact with LMAs. With the employment of this protective strategy, the interfacial reactions and degradation are suppressed, leading to the chemical stability of PTV-SPE toward LMAs.

2.4. Practical Application of the Side-Chain-Anchored Polymer Electrolyte. To further demonstrate the practical application of PTV-SPE, full cells were assembled to investigate the charge/discharge performance. The assembled $LiFePO_4$ (LFP)/PTV-SPE/Li cell achieves an initial discharge specific capacity of 147.5 mAh g^{-1} at 1 C and exhibits a high capacity retention of 80.0% beyond 960 cycles (Figure 6a). In contrast, the PVC-based cell has only 401 cycles at 80.0% capacity retention and exhibits an inferior average Coulomb efficiency owing to the deteriorating interfacial side reactions. Meanwhile, the PTV-based cell exhibited an initial Coulombic efficiency of 89.1%, higher than 86.6% of the PVC-based cell. Moreover, the PTV-based cell also possesses a longer cycle number compared to that of reported PVC-based cells, which is attributed to the improved stability of the polymer by the formation of the restricted conformation via anchoring side chains (Figure 6b). In addition, the rate performance of the LFP/Li cells was measured from 0.2 to 6 C. The cell of PTV-SPE exhibits a stable discharge specific capacity of 158.1 mAh g^{-1} at 0.2 C and delivers better rate performance than that of PVC-SPE (87.3 vs 62.1 mAh g^{-1}) at 6 C (Figure 6c), which can be supported by the lower polarization and stable discharge capacity of PTV-SPE at high rates (Figure S20). To investigate the high-voltage performance of PTV-SPE, $LiNi_{0.8}Co_{0.1}Mn_{0.1}O_2$ (NCM811)/Li cells were assembled and

https://doi.org/10.1021/jacs.5c00760
J. Am. Chem. Soc. 2025, 147, 16154−16163

evaluated. The result of the electrochemical float analysis shows unstable leakage currents for PVC-SPE measured at 4.5 V (Figure 6d). In contrast, no leakage current (less than 0.1 mA) is observed in PTV-SPE at 4.7 V, suggesting that PTV-SPE has better stability at high voltage. For long-term storage, the PTV-based cell charged to 4.3 V exhibits a self-discharge of 1.0% capacity decay after storage for 24 h, outperforming the PVC-based cell of 8.7% per day (Figure 6e). The lower level of self-discharge at storage suggests that PTV-SPE possesses higher polymer stability and interfacial stability attributed to the design strategy of the restricted conformation. As a result, the developed 4.3 V PTV-based cell renders a high capacity retention rate of 78.0% at 300 cycles compared to the capacity retention rate of 77.5% at 130 cycles for the PVC-SPE (Figure 6f). To further demonstrate the practicability of PTV-SPE, practical 0.8 Ah multilayer pouch cells were assembled with commercial-level LMAs and NCM811 cathodes. It is observed that the PTV-based pouch cell can run the fan efficiently (Figure 6g). Furthermore, the PTV-based pouch cell also exhibits superior cycling stability with a capacity retention of 86.8% after 60 cycles at 0.5 C and room temperature, which is far superior to the capacity retention of the PVC-based pouch cell, demonstrating great potential for practical applications of PTV-SPE (Figure 6h).

3. CONCLUSIONS

We present a facile strategy to effectively suppress the interfacial degradation of polycarbonate-based solid polymer electrolytes via in situ anchoring of protective side chains into polycarbonate-based electrolytes. This strategy enables the side chains forming restricted conformation to shield the degradable ester bonds of cyclic carbonate structures through hydrogen-bonding anchoring, suppressing the interfacial degradation of the fragile structures of Li^+ transport. This unique design improves the anodic chemical stability of cyclic carbonate structures, enabling stable Li plating/stripping of the PTV-based symmetrical cell beyond 1000 h at a current density of 0.5 mA cm^{-2}. In addition, the corresponding full cell also demonstrates a stable cycling capability of over 1000 cycles, and the practical pouch cell with a capacity of 0.8 Ah also shows a stable cycling performance. This work showcases a feasible avenue toward manufacturing highly stable polycarbonate-based solid-state LMBs.

■ ASSOCIATED CONTENT

Supporting Information

The Supporting Information is available free of charge at https://pubs.acs.org/doi/10.1021/jacs.5c00760.

Detailed materials, experimental procedures, characterization methods, computational simulations, and supporting figures (PDF)

■ AUTHOR INFORMATION

Corresponding Authors

Chaobin He − *Department of Materials Science and Engineering, National University of Singapore, Singapore 117574, Singapore; Institute of Materials Research and Engineering, Agency for Science, Technology and Research, A*STAR, Singapore 138634, Singapore;* orcid.org/0000-0001-8200-8337; Email: msehc@nus.edu.sg

Lin Xu − *State Key Laboratory of Advanced Technology for Materials Synthesis and Processing, School of Materials Science and Engineering, Wuhan University of Technology, Wuhan 430070, P. R. China; Hubei Longzhong Laboratory, Wuhan University of Technology (Xiangyang Demonstration Zone), Xiangyang 441000 Hubei, P. R. China; Hainan Institute, Wuhan University of Technology, Sanya 572000, P. R. China; Zhongyu Feima New Material Technology Innovation Center (Zhengzhou) Co., Ltd., Zhengzhou 450001, P. R. China;* orcid.org/0000-0003-2347-288X; Email: linxu@whut.edu.cn

Authors

Hantao Xu − *State Key Laboratory of Advanced Technology for Materials Synthesis and Processing, School of Materials Science and Engineering, Wuhan University of Technology, Wuhan 430070, P. R. China; Department of Materials Science and Engineering, National University of Singapore, Singapore 117574, Singapore*

Wei Deng − *State Key Laboratory of Advanced Technology for Materials Synthesis and Processing, School of Materials Science and Engineering, Wuhan University of Technology, Wuhan 430070, P. R. China*

Jingyuan Yu − *State Key Laboratory of Advanced Technology for Materials Synthesis and Processing, School of Materials Science and Engineering, Wuhan University of Technology, Wuhan 430070, P. R. China*

Lei Shi − *State Key Laboratory of Advanced Technology for Materials Synthesis and Processing, School of Materials Science and Engineering, Wuhan University of Technology, Wuhan 430070, P. R. China*

Wenwei Zhang − *State Key Laboratory of Advanced Technology for Materials Synthesis and Processing, School of Materials Science and Engineering, Wuhan University of Technology, Wuhan 430070, P. R. China*

Juncai Long − *State Key Laboratory of Advanced Technology for Materials Synthesis and Processing, School of Materials Science and Engineering, Wuhan University of Technology, Wuhan 430070, P. R. China;* orcid.org/0009-0007-6342-597X

Complete contact information is available at: https://pubs.acs.org/10.1021/jacs.5c00760

Author Contributions

[▽]H.X., W.D., and J.Y. contributed equally to this work.

Notes

The authors declare no competing financial interest.

■ ACKNOWLEDGMENTS

This work was supported by the National Natural Science Foundation of China (52272234), the National Key Research and Development Program of China (2020YFA0715000), the International Science and Technology Cooperation Program of Hubei Province (2024EHA039), and the Independent Innovation Project of Hubei Longzhong Laboratory (2022ZZ-20). Chaobin He would like to thank NRF Singapore for funding support (CRP30-2023-0032). Hantao Xu would like to acknowledge financial support from China Scholarship Council (202406950069).

■ REFERENCES

(1) Zhang, W.; Sayavong, P.; Xiao, X.; Oyakhire, S. T.; Shuchi, S. B.; Vilá, R. A.; Boyle, D. T.; Kim, S. C.; Kim, M. S.; Holmes, S. E.; Ye, Y.; Li, D.; Bent, S. F.; Cui, Y. Recovery of isolated lithium through discharged state calendar ageing. *Nature* **2024**, *626* (7998), 306−312.

(2) Jie, Y.; Wang, S.; Weng, S.; Liu, Y.; Yang, M.; Tang, C.; Li, X.; Zhang, Z.; Zhang, Y.; Chen, Y.; Huang, F.; Xu, Y.; Li, W.; Guo, Y.; He, Z.; Ren, X.; Lu, Y.; Yang, K.; Cao, S.; Lin, H.; Cao, R.; Yan, P.; Cheng, T.; Wang, X.; Jiao, S.; Xu, D. Towards long-life 500 Wh kg^{-1} lithium metal pouch cells via compact ion-pair aggregate electrolytes. *Nat. Energy* **2024**, *9* (8), 987−998.
(3) Guo, R.; Zhang, K.; Zhao, W.; Hu, Z.; Li, S.; Zhong, Y.; Yang, R.; Wang, X.; Wang, J.; Wu, C.; Bai, Y. Interfacial Challenges and Strategies toward Practical Sulfide-Based Solid-State Lithium Batteries. *Energy Mater. Adv.* **2023**, *4*, No. 0022.
(4) Wang, Z.; Zhao, J.; Zhang, X.; Rong, Z.; Tang, Y.; Liu, X.; Zhu, L.; Zhang, L.; Huang, J. Tailoring lithium concentration in alloy anodes for long cycling and high areal capacity in sulfide-based all solid-state batteries. *eScience* **2023**, *3* (1), No. 100087.
(5) Zhang, X.; Chen, S.; Zhu, J.; Gao, Y. A Critical Review of Thermal Runaway Prediction and Early-Warning Methods for Lithium-Ion Batteries. *Energy Mater. Adv.* **2023**, *4*, No. 0008.
(6) Han, S.; Wen, P.; Wang, H.; Zhou, Y.; Gu, Y.; Zhang, L.; Shao-Horn, Y.; Lin, X.; Chen, M. Sequencing polymers to enable solid-state lithium batteries. *Nat. Mater.* **2023**, *22* (12), 1515−1522.
(7) Yang, L.; Zhang, H.; Xu, H.; Peng, W.; Wu, L.; Cheng, Y.; Liu, Y.; Xu, L.; Mai, L. Interfacial Catalysis Strategy for High-Performance Solid-State Lithium Metal Batteries. *Adv. Energy Mater.* **2024**, *14*, No. 2401829.
(8) Lyu, W.; Fu, H.; Rao, A. M.; Lu, Z.; Yu, X.; Lin, Y.; Zhou, J.; Lu, B. Permeable void-free interface for all-solid-state alkali-ion polymer batteries. *Sci. Adv.* **2024**, *10* (42), No. eadr9602.
(9) Wu, Q.; Fang, M.; Jiao, S.; Li, S.; Zhang, S.; Shen, Z.; Mao, S.; Mao, J.; Zhang, J.; Tan, Y.; Shen, K.; Lv, J.; Hu, W.; He, Y.; Lu, Y. Phase regulation enabling dense polymer-based composite electrolytes for solid-state lithium metal batteries. *Nat. Commun.* **2023**, *14* (1), 6296.
(10) Zhou, Y.-N.; Yong, H.; Guo, R.; Wang, K.; Li, Z.; Hua, W.; Zhou, D. Self-reporting and Biodegradable Thermosetting Solid Polymer Electrolyte. *Angew. Chem., Int. Ed.* **2024**, *63* (7), No. e202319003.
(11) Yang, J.; Cao, Z.; Chen, Y.; Liu, X.; Xiang, Y.; Yuan, Y.; Xin, C.; Xia, Y.; Huang, S.; Qiang, Z.; Fu, K. K.; Zhang, J. Dry-Processable Polymer Electrolytes for Solid Manufactured Batteries. *ACS Nano* **2023**, *17* (20), 19903−19913.
(12) Wang, H.; Yang, Y.; Gao, C.; Chen, T.; Song, J.; Zuo, Y.; Fang, Q.; Yang, T.; Xiao, W.; Zhang, K.; Wang, X.; Xia, D. An entanglement association polymer electrolyte for Li-metal batteries. *Nat. Commun.* **2024**, *15* (1), 2500.
(13) An, Y.; Han, X.; Liu, Y.; Azhar, A.; Na, J.; Nanjundan, A. K.; Wang, S.; Yu, J.; Yamauchi, Y. Progress in Solid Polymer Electrolytes for Lithium-Ion Batteries and Beyond. *Small* **2022**, *18* (3), No. 2103617.
(14) Didwal, P. N.; Singhbabu, Y. N.; Verma, R.; Sung, B.-J.; Lee, G.-H.; Lee, J.-S.; Chang, D. R.; Park, C.-J. An advanced solid polymer electrolyte composed of poly(propylene carbonate) and mesoporous silica nanoparticles for use in all-solid-state lithium-ion batteries. *Energy Storage Mater.* **2021**, *37*, 476−490.
(15) Dong, T.; Zhang, H.; Hu, R.; Mu, P.; Liu, Z.; Du, X.; Lu, C.; Lu, G.; Liu, W.; Cui, G. A rigid-flexible coupling poly(vinylene carbonate) based cross-linked network: A versatile polymer platform for solid-state polymer lithium batteries. *Energy Storage Mater.* **2022**, *50*, 525−532.
(16) Lu, X.; Wang, Y.; Xu, X.; Yan, B.; Wu, T.; Lu, L. Polymer-Based Solid-State Electrolytes for High-Energy-Density Lithium-Ion Batteries−Review. *Adv. Energy Mater.* **2023**, *13* (38), No. 2301746.
(17) Rosenbach, D.; Krimalowski, A.; Erabhoina, H.; Thelakkat, M. Solid polymer electrolytes from polyesters with diester sidechains for lithium metal batteries. *J. Mater. Chem. A* **2022**, *10* (16), 8932−8947.
(18) Zhang, J.; Yang, J.; Dong, T.; Zhang, M.; Chai, J.; Dong, S.; Wu, T.; Zhou, X.; Cui, G. Aliphatic Polycarbonate-Based Solid-State Polymer Electrolytes for Advanced Lithium Batteries: Advances and Perspective. *Small* **2018**, *14* (36), No. 1800821.
(19) Xiao, G.; Xu, H.; Bai, C.; Liu, M.; He, Y.-B. Progress and perspectives of in situ polymerization method for lithium-based batteries. *Interd. Mater.* **2023**, *2* (4), 609−634.
(20) Xu, H.; Deng, W.; Shi, L.; Long, J.; Zhang, Y.; Xu, L.; Mai, L. The Role of the Molecular Encapsulation Effect in Stabilizing Hydrogen-Bond-Rich Gel-State Lithium Metal Batteries. *Angew. Chem., Int. Ed.* **2024**, *63* (27), No. e202400032.
(21) Wang, C.; Zhang, H.; Li, J.; Chai, J.; Dong, S.; Cui, G. The interfacial evolution between polycarbonate-based polymer electrolyte and Li-metal anode. *J. Power Sources* **2018**, *397*, 157−161.
(22) Brennan, M. D.; Breedon, M.; Best, A. S.; Morishita, T.; Spencer, M. J. S. Surface Reactions of Ethylene Carbonate and Propylene Carbonate on the Li(001) Surface. *Electrochim. Acta* **2017**, *243*, 320−330.
(23) Xu, H.; Zhang, H.; Ma, J.; Xu, G.; Dong, T.; Chen, J.; Cui, G. Overcoming the Challenges of 5 V Spinel LiNi0.5Mn1.5O4 Cathodes with Solid Polymer Electrolytes. *ACS Energy Lett.* **2019**, *4* (12), 2871−2886.
(24) Chai, J.; Liu, Z.; Ma, J.; Wang, J.; Liu, X.; Liu, H.; Zhang, J.; Cui, G.; Chen, L. In Situ Generation of Poly (Vinylene Carbonate) Based Solid Electrolyte with Interfacial Stability for LiCoO2 Lithium Batteries. *Adv. Sci.* **2016**, *4* (2), No. 1600377.
(25) Zhang, M.; Lei, C.; Zhou, T.; Song, S.; Paoprasert, P.; He, X.; Liang, X. Segmental Motion Adjustment of the Polycarbonate Electrolyte for Lithium-Metal Batteries. *ACS Appl. Mater. Interfaces* **2022**, *14* (50), 55653−55663.
(26) Guo, Y.; Pan, S.; Yi, X.; Chi, S.; Yin, X.; Geng, C.; Yin, Q.; Zhan, Q.; Zhao, Z.; Jin, F.-M.; Fang, H.; He, Y.-B.; Kang, F.; Wu, S.; Yang, Q.-H. Fluorinating All Interfaces Enables Super-Stable Solid-State Lithium Batteries by In Situ Conversion of Detrimental Surface Li_2CO_3. *Adv. Mater.* **2024**, *36* (13), No. 2308493.
(27) Yao, W.; He, S.; Xu, J.; Wang, J.; He, M.; Zhang, Q.; Li, Y.; Xiao, X. Polypyrrole Nanotube Sponge Host for Stable Lithium-Metal Batteries under Lean Electrolyte Conditions. *ACS Sustain. Chem. Eng.* **2021**, *9* (6), 2543−2551.
(28) Li, X.; Li, M.; Liu, Y.; Jie, Y.; Li, W.; Chen, Y.; Huang, F.; Zhang, Y.; Sohail, T. M.; Wang, S.; Zhu, X.; Cheng, T.; Gu, M. D.; Jiao, S.; Cao, R. Fast Interfacial Defluorination Kinetics Enables Stable Cycling of Low-Temperature Lithium Metal Batteries. *J. Am. Chem. Soc.* **2024**, *146* (25), 17023−17031.
(29) Hu, R.; Qiu, H.; Zhang, H.; Wang, P.; Du, X.; Ma, J.; Wu, T.; Lu, C.; Zhou, X.; Cui, G. A Polymer-Reinforced SEI Layer Induced by a Cyclic Carbonate-Based Polymer Electrolyte Boosting 4.45 V $LiCoO_2$/Li Metal Batteries. *Small* **2020**, *16* (13), No. 1907163.
(30) Xu, H.; Yang, J.; Niu, Y.; Hou, X.; Sun, Z.; Jiang, C.; Xiao, Y.; He, C.; Yang, S.; Li, B.; Chen, W. Deciphering and Integrating Functionalized Side Chains for High Ion-Conductive Elastic Ternary Copolymer Solid-State Electrolytes for Safe Lithium Metal Batteries. *Angew. Chem., Int. Ed.* **2024**, *63* (36), No. e202406637.
(31) Meyers, G. F.; Hall, M. B.; Chinn, J. W., Jr.; Lagow, R. J. X-ray photoelectron spectra of methyllithium and dilithiomethane. *J. Am. Chem. Soc.* **1985**, *107* (5), 1413−1414.
(32) Zhao, Q.; Liu, X.; Stalin, S.; Khan, K.; Archer, L. A. Solid-state polymer electrolytes with in-built fast interfacial transport for secondary lithium batteries. *Nat. Energy* **2019**, *4* (5), 365−373.
(33) Mafy, N. N.; Afrin, T.; Rahman, M. M.; Mollah, M. Y. A.; Susan, M. A. B. H. Effect of temperature perturbation on hydrogen bonding in aqueous solutions of different urea concentrations. *RSC Adv.* **2015**, *5* (73), 59263−59272.
(34) Joris, L.; Schleyer, P. V. R. Hydrogen bonding. XIX. Intramolecular hydrogen bonding in aliphatic hydroxy ketones. *J. Am. Chem. Soc.* **1968**, *90* (17), 4599−4611.
(35) Lu, W.; Sun, L.; Zhao, Y.; Wu, T.; Cong, L.; Liu, J.; Liu, Y.; Xie, H. Elongating the cycle life of lithium metal batteries in carbonate electrolyte with gradient solid electrolyte interphase layer. *Energy Storage Mater.* **2021**, *34*, 241−249.
(36) Zhang, Y.; Chen, S.; Chen, Y.; Li, L. Functional polyethylene glycol-based solid electrolytes with enhanced interfacial compatibility

for room-temperature lithium metal batteries. *Mater. Chem. Front.* **2021**, *5* (9), 3681−3691.
(37) Huang, X.; Wu, J.; Wang, X.; Tian, Y.; Zhang, F.; Yang, M.; Xu, B.; Wu, B.; Liu, X.; Li, H. In Situ Synthesis of a $Li_{6.4}La_3Zr_{1.4}Ta_{0.6}O_{12}$/Poly(vinylene carbonate) Hybrid Solid-State Electrolyte with Enhanced Ionic Conductivity and Stability. *ACS Appl. Energy Mater.* **2021**, *4* (9), 9368−9375.
(38) Zheng, F.; Li, H.-T.; Zheng, Y.-Z.; Wang, D.; Yang, N.-N.; Ding, H.-Y.; Tao, X. Trimethyl phosphate-enhanced polyvinyl carbonate polymer electrolyte with improved interfacial stability for solid-state lithium battery. *Rare Metals* **2022**, *41* (6), 1889−1898.
(39) Ma, C.; Feng, Y.; Xing, F.; Zhou, L.; Yang, Y.; Xia, Q.; Zhou, L.; Zhang, L.; Chen, L.; Ivey, D. G.; Sadoway, D. R.; Wei, W. A borate decorated anion-immobilized solid polymer electrolyte for dendrite-free, long-life Li metal batteries. *J. Mater. Chem. A* **2019**, *7* (34), 19970−19976.
(40) Tian, C.; Song, M.; Tang, J.; Yuan, H.; Ai, C.; Cao, H.; Huang, T.; Yu, A. Rational Design of a Cross-Linked Composite Solid Electrolyte for Li-Metal Batteries. *ACS Appl. Mater. Interfaces* **2024**, *16* (1), 1535−1542.
(41) Jin, Y.; Lin, R.; Li, Y.; Zhang, X.; Tan, S.; Shuai, Y.; Xiong, Y. Revealing the Influence of Electron Migration Inside Polymer Electrolyte on Li+ Transport and Interphase Reconfiguration for Li Metal Batteries. *Angew. Chem., Int. Ed.* **2024**, *63* (24), No. e202403661.
(42) Zuo, J.; Dang, Y.; Zhai, P.; Li, B.; Wang, L.; Wang, M.; Yang, Z.; Chen, Q.; Gu, X.; Li, Z.; Tang, P.; Gong, Y. Fast Lithium Ion Transport Pathways Constructed by Two-Dimensional Boron Nitride Nanoflakes in Quasi-Solid-State Polymer Electrolyte. *Nano Lett.* **2023**, *23* (17), 8106−8114.
(43) Peng, H.; Long, T.; Peng, J.; Chen, H.; Ji, L.; Sun, H.; Huang, L.; Sun, S.-G. Molecular Design for In-Situ Polymerized Solid Polymer Electrolytes Enabling Stable Cycling of Lithium Metal Batteries. *Adv. Energy Mater.* **2024**, *14* (22), No. 2400428.

https://doi.org/10.1021/jacs.5c00760
J. Am. Chem. Soc. 2025, 147, 16154−16163